JETIR.ORG ISSN: 2349-5162 | ESTD Year : 2014 | Monthly Issue
JOURNAL OF EMERGING TECHNOLOGIES AND INNOVATIVE RESEARCH (JETIR)
An International Scholarly Open Access, Peer-reviewed, Refereed Journal

CFD Modelling Design of hydrate formation on raw natural gas pipelines in oil and gas industry

Ibe Raymond Obinna, Nnadikwe Johnson, Nabila Hagouch.

Abstract

The oil and gas industry's flow assurance programs are hampered by gas hydrates. This study focuses on the mechanisms of hydrate formation in natural gas pipelines. The mechanics of water vapour condensation and subsequent water accumulation in lowered parts of a gas pipeline were studied using Computational Fluid Dynamics (CFD). The pipeline temperature profile, condensation of water vapour at walls, hydrate production, and hydrate slurry rheology were all modeled using user defined functions (UDF) incorporated into the CFD software Fluent. Water buildup and hydrate formation were discovered naturally in the uphill sections of gas pipes. CFD has been proved to be an effective technique for deciphering complex physical processes in multiphase flow conditions.

Keywords: natural gas, pipelines, condensation, hydrate formation, uphill sections, viscosity, nucleation, sagging sections, kinetics, macroscopic.

1 Introduction

Gas producers are constantly under pressure to operate at higher pressures due to rising energy demand. At the turn of the twentieth century, the natural gas industry began to experience unanticipated pipeline obstructions. In 1934, Hammer Schmidt demonstrated that the ice-like obstructions were actually gas hydrates. The formation of gas hydrates in oil and gas pipelines is an unwelcome occurrence that jeopardizes flow assurance procedures while also endangering workers and equipment. Clathrate hydrates are non-stoichiometric water-natural-gas mixtures with gas molecules trapped in a polygonal crystalline structure made up of water molecules. The water molecules form an ordered ring around the gas molecules, entrapping them. These gas hydrates have the appearance of ice, yet under high pressures, they can develop much above the freezing point of water.

The formation of hydrates in natural gas pipes is a complicated process. The events that lead to hydrate development in gas pipelines are water vapor condensation, accumulation of water at lower regions of the pipeline, nucleation and growth of hydrate particles, and eventually pipeline obstruction. Because the hydrate that has just been released from the pipewall along the length of the pipeline may migrate downstream and deposit at sagging areas of the pipeline to cause the blockage at the start of summer, the location of the pipeline blockage may not be the same as the location of hydrate deposition. Due to the enormity of the problem and the enormous pressures involved, experiments on natural gas hydrate in pipelines under real-world conditions are

difficult to repeat. Different experimenters, on the other hand, have focused on different aspects of hydrate formation. The formation and breakdown dynamics of gas hydrates were addressed at a conceptual level by Bishoni et al., emphasizing the numerous stages of hydrate formation and evolution. Riberio et al. conducted a thorough review of the literature on hydrate formation dynamics, highlighting various researchers' modeling efforts. ExxonMobil Upstream Research Company and Tulsa University collaborated to set up industrial scale flow loop tests to mimic genuine hydrate formation requirements, and Davies et al. proved their hydrate formation model against the experimental data. While the hydrate formation scenario just presented was for oil-dominated flowlines, hydrate formation in natural gas pipelines could be substantially different.

Theory

Natural gas pipelines always have some moisture content because the gas from the formations reaches the well head saturated with water. Ground temperatures are lower during the winter, causing the temperature of the pipeline content to drop. When the temperature of the gas falls below the saturation temperature, which corresponds to the dew point of water, condensation of water vapors occurs. Condensate collects near the pipe's base in straighter sections of the pipeline due to gravity. The collection may increase near the sagging/uphill sections of the pipe. When there is enough water present and the thermodynamic conditions are favorable, hydrate nucleation processes begin. In theory, hydrate formation can be studied using either one-dimensional (1-D) or three-dimensional (3-D) models. While 1-D CFD models are appropriate for very long pipeline sections, 3-D CFD approaches are required to model the effects of water condensation and accumulation.

2 CFD model

As an application example, the pipeline portion shown in Figure 1 was chosen. Around 84000 polyhedral control volumes make up the computational domain. The grid was updated during the computational run time to resolve the accumulating problem.

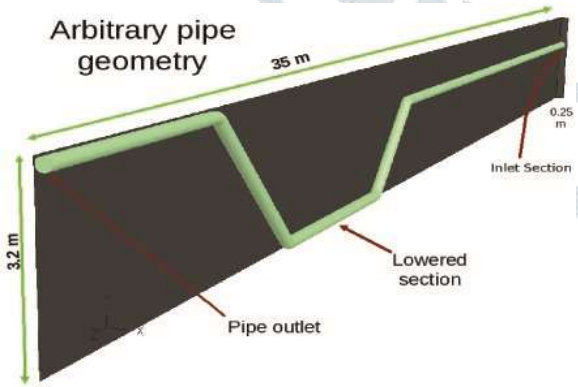

Figure 1: Natural gas pipeline.

Fluent's "Mixture Model" was used to represent the interpenetrating continuum made up of mixture components.

Table 1: Model parameters.

No.	Model parameter	Value
1.	Pipe diameter	0.25m
2.	Inlet velocity	2m/s

3.	Water vapor volume fraction	0.2
4.	Inlet temperature	315K
5.	Operating pressure	6.3Mpa

Table 1 displays various pipeline section parameters. To connect the pressure and velocity fields, the Pressure Implicit Split Operator (PISO) algorithm was utilized. To simulate the effects of turbulence, the K-Epsilon model was used.

2.1 Mathematical framework

Table 1 displays various pipeline section parameters. To connect the pressure and velocity fields, the Pressure Implicit Split Operator (PISO) algorithm was utilized. To simulate the effects of turbulence, the K-Epsilon model was used.

Continuity:

$$\frac{\partial}{\partial t}(\rho_m) + \nabla \cdot (\rho_m \vec{v}_m) = 0 \qquad (1)$$

Momentum:

$$\frac{\partial}{\partial t}(\rho_m \vec{v}_m) + \nabla \cdot (\rho_m \vec{v}_m \vec{v}_m) = \nabla p + \nabla \cdot \left[\mu_m \left(\nabla \vec{v_m} + \nabla \vec{v_m^T}\right) + \rho_m \vec{g}, \right.$$
$$\left. + \vec{F} + \nabla \cdot \left(\sum_{k=1}^{n} \alpha_k \rho_k \vec{v}_{dr,k} \vec{v}_{dr,k}\right) \right. \qquad (2)$$

Energy:

$$\frac{\partial}{\partial t}\sum_{k=1}^{n}(\alpha_k \rho_k E_k) + \nabla \cdot \sum_{k=1}^{n}(\alpha_k \vec{v}_k (\rho_k E_k + p)) = \nabla \cdot [k_{eff} \nabla T] + S_E \qquad (3)$$

Where $\vec{v}_m$ is the mass averaged velocity, ρ_m and μ_m are volume fraction averaged mixture density and viscosity respectively, $\vec{v}_{dr,k}$ is the drift velocity of individual phases, E_k is the energy of phase k, α_k represents the volume fraction of phase k, p represents pressure, k_{eff} is the effective thermal conductivity, T represents the temperature and S_E represents energy source. A drift flux model available in Fluent was used to model the drag of the primary phase on the secondary phases, where the slip velocity was modelled as described by Minnan et al. and the drag function correlation of Schiller and Neumann was employed.

2.2 Model setup

For the purposes of this investigation, a certain composition of natural gas was assumed at the pipe's entrance. The molar concentrations were fed into the program 'CSM Hyd', which produced a pressure-temperature equilibrium curve for hydrate production. An equation reflecting the threshold temperature for hydrate formation was obtained based on the best fit via the equilibrium data

$$T = 8.5274 \times \ln(P) + 270.86 \qquad (4)$$

Where T denotes temperature in Kelvin and P denotes pressure in millipascals. The following equation was used to compute the saturation temperature based on the partial pressure of vapor.

$$T_{sat} = 16.335 \times \ln(P) + 167.08 \quad (5)$$

A connection discovered by De Schepper et al. [11,12] was used to appropriately model condensation in Fluent.

$$M_{water} = 0{\cdot}1 \times \alpha vapour \times \rho vapour |Tsat - Twall|/T_{sat} \quad (6)$$

Modeling the temperature profile of the pipeline content along the length of the buried pipeline is a difficult issue since it fluctuates with seasonal changes as well as local changes in the conditions near the pipeline. To represent the temperature profile of the pipe along its length, a simple formula was utilized.

$$T(x) = T_{Gr} + (T_o - T_{Gr}) \exp\left(\frac{-k\pi Dx}{0.28QC_p}\right) \quad (7)$$

where T_{Gr} is the ground temperature, x is the distance along the pipe from the inlet, D is the pipe diameter, k is thermal conductivity, Q is the volumetric flow rate and C_p is the specific heat capacity.

The kinetic modeling of hydrate nucleation and growth requires the defining of a driving force. Despite the fact that numerous scholars have presented their own versions of kinetic models, there is a widespread lack of unanimity. These models' applicability to dynamic flow systems is limited by assumptions about molecular thermodynamics as well as experimental setup constraints. The work of Kashchiev and Firoozabadi, who employed the difference in chemical potential of the species as a driving factor, is one of the most well-known. The gap between the microscopic phenomenon of crystallization and its macroscopic ramifications can be bridged using an appropriate kinetic model. The premise is that instantaneous nucleation occurs due to a large number of nucleation sites (due to pipe wall roughness) and a high supersaturation of the condensed liquid water layer on the pipe wall with hydrocarbon gas under high pressure. Based on the normal stoichiometric molar relationship for hydrate formation, the threshold mass fraction (considering water and hydrocarbon gas) in a cell was set to roughly 0.866. The UDFs were used to set this value as a threshold.

When hydrate formation conditions are satisfied in a computational cell, mass transfer equations for both phases, namely water and gas, are used to model the hydrate formation using the simplified relationship shown below:

$$Mhyd = (\rho water \times \alpha water) + (\rho gas \times \alpha gas) \quad (8)$$

The following relationship [10,15] was utilized to incorporate the rheological effects of increasing suspension in the solution:

$$\mu slurry = \alpha water\ (1 - \alpha hyd)^{-2.5} \quad (9)$$

3 Results and discussion

The effect of water condensation on the pipe walls and buildup at the bottom of the pipe section is depicted in Figure 2. Condensed water begins to form at the bottom of the pipe, at the 6 o'clock position, and flows in the mean flow direction when water vapor condensation begins. This effect is depicted in Figure 2. It is stated that the accumulating effect can only be noticed in three-dimensional simulations and that one-dimensional models ignore it altogether. In addition, the collecting of free water at the uphill end of the pipe is depicted.

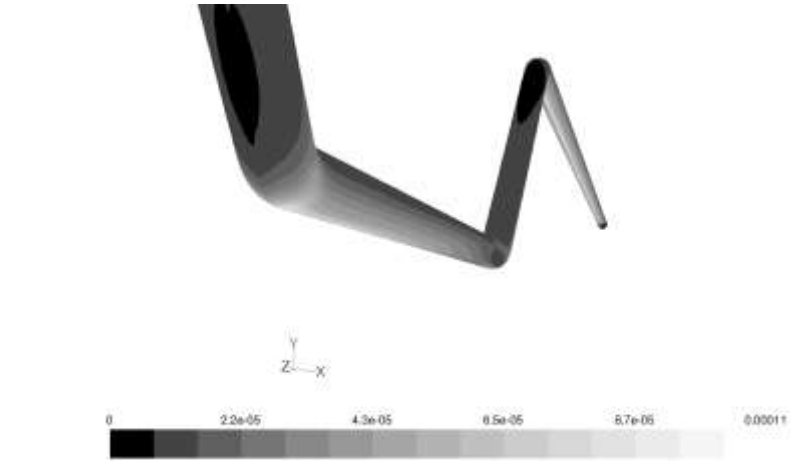

Figure 2: Water phase contours showing condensation at wall and accumulation at the bottom of the pipe.

Water accumulation in pipelines due to gravity is known to have two basic mechanisms: accumulation at the pipe's bottom and accumulation at the base of uphill/sagging regions of the pipe. Figure 2 shows the accumulation phenomena, which is a compound effect that happens at the base of the uphill part of the pipe for the reasons indicated above.

The existence of free water, according to Sloan, is a crucial factor in the onset of hydrate formation. According to the simulation, hydrate nucleation is especially sensitive near the base of drooping pipeline sections because these locations operate as stagnation points/traps for any condensed water in gas flows. In certain places, hydrate development could start in the winter. Several hydrate deposits along the pipe's length cause an increase in pressure drop. The biggest issue may come at the start of summer, when the hydrate loosens up (but is not completely dissociated) at the pipeline walls and begins to move. The hydrate that has been sloughed off then flows in the direction of the mean flow until it reaches lowered areas, where it becomes stuck as packed deposits. The location of high hydrate volume % in accumulated water is depicted in Figure 3. hydrate concentration isosurfaces that can be separated from water isosurfaces define the high hydrate volume fraction zone. Water stagnation points are obviously the most prone to hydrate generation. Hydrate formation provides as added resistance to flow, as shown by the velocity vectors in the cut-plane across x = 0. The velocity vectors depicted at x = 0 iso-plane are shifted by some distance for better visibility. A standstill zone with high hydrate volume fraction regions can be seen. The velocity difference between the mean flow and the hydrate deposits would generate a drag force between phases in real pipelines, causing pressure loss and jeopardizing flow assurance.

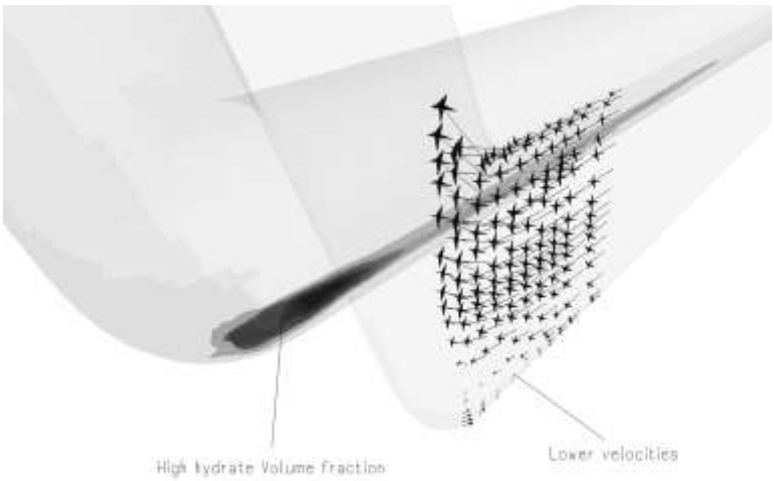

Figure 3: Velocity vectors at x=0 plane drawn at an offset showing the effect of high hydrate concentration.

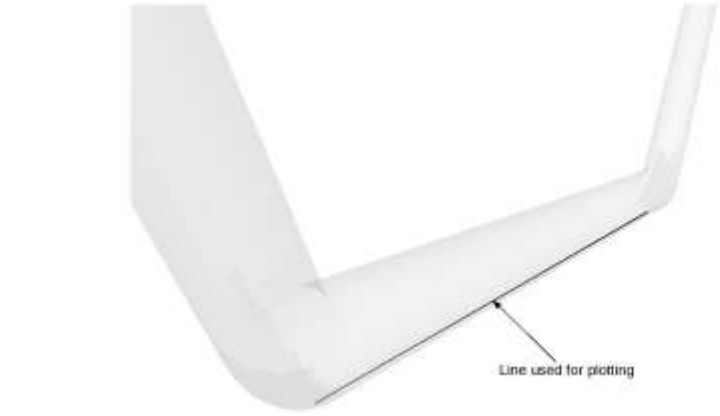

Figure 4: Line used for the plots.

To plot different characteristics, a line was drawn directly below the bottom of the lowered part of the pipe, between sections 22m and 28m (measured from the inlet), as shown in figure 4.

The fluctuation in viscosity and water volume fraction at the base of the lowered (straight) portion is depicted in Figure 5. The gradual increase in viscosity mixture defined as $\mu_m = \sum_{k=1}^{n} \alpha_k \mu_k$ goes hand in hand with an increase in the water volume fraction, with a sharp spike suggesting a high hydrate volume fraction impacting the viscosity of the mixture The gradual slope of the curve before 27m emphasizes the water collection phenomenon (pileup). The abrupt increase in viscosity

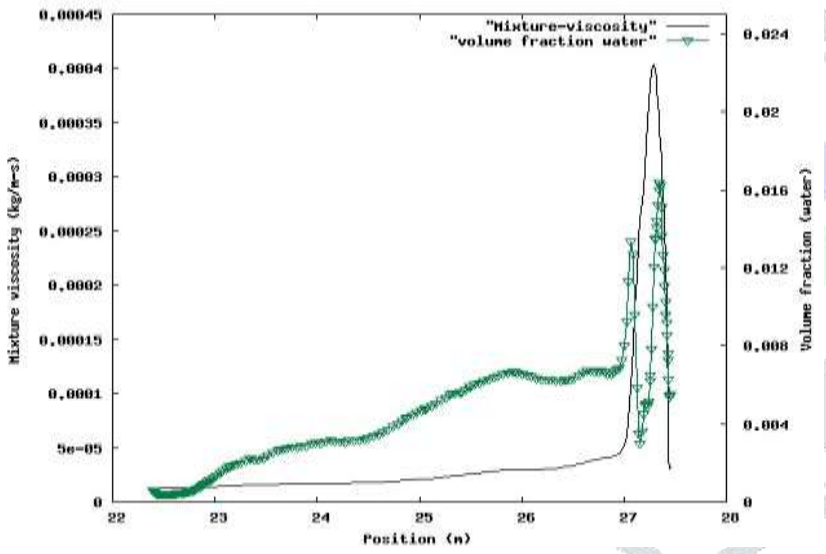

Figure 5: Mixture viscosity and water volume fraction along the length of lowered section of the pipe. beyond 27m indicates the creation of a new phase, which has a significant impact on the viscosity of the mixture.

The water volume fraction is depicted in Figure 5 as a steady increase, followed by a sharp increase, a sharp fall, and still another sharp increase. The steep decline occurs at a zone with a high hydrate volume %, acting as a "double-sided tidal barrage" between downstream and upstream water. It's fascinating to see how hydrate deposition influences the water film traveling in the direction of the mean flow. On the upstream side of the deposit, it acts as a wall, creating an increase in water volume as shown in the image, while on the downstream side, it acts as a sandbag, as shown in the image. The backflow of a water film near to the deposit causes water buildup. Backflow is aided by dynamic pressure loss in the deposit-shadowed region and gravity effects in the uphill part.

The mixture velocity $\vec{v_m} = \sum_{k=1}^{n} \alpha_k \rho_k \vec{v_k} / \rho_m$ at the bottom of the pipe section is shown in figure 6. The rise in velocity between 22–22.5m is caused by mean flow from the downhill part impinging on the wall, causing the

velocity to increase. The velocity of the mixture decreases beyond 22.5m due to friction at the walls. The mixing velocity oscillates with a mean value of roughly 0.5m/s in the region between 23–26m. Beyond 27m, the "fish-hook" curve reveals a substantial decline in mixture velocity due to a high hydrate volume fraction.

Figure 7 depicts the variation of static and dynamic pressure. The dramatic increase in static pressure (and drop in dynamic pressure) at approximately 27m illustrates the impact of significant hydrate deposition.

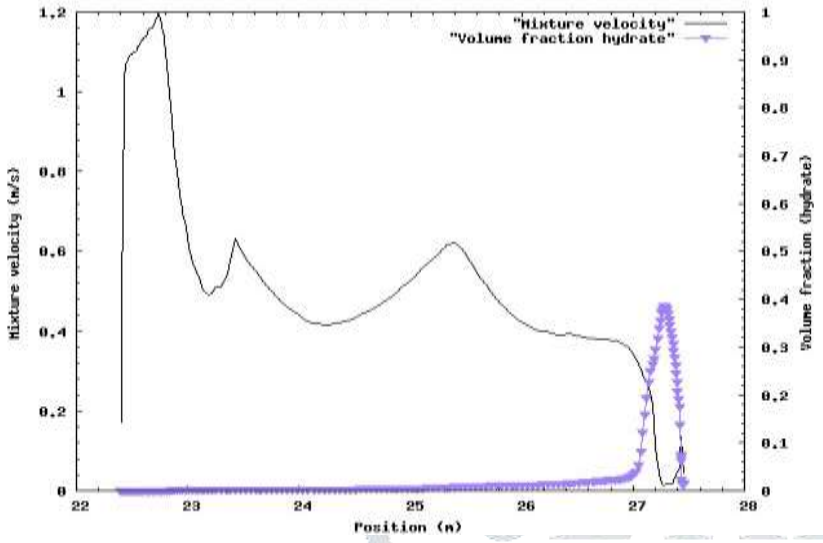

Figure 6: Mixturevelocityand hydratevolumefractionalong the lengthof lowered section of the pipe.

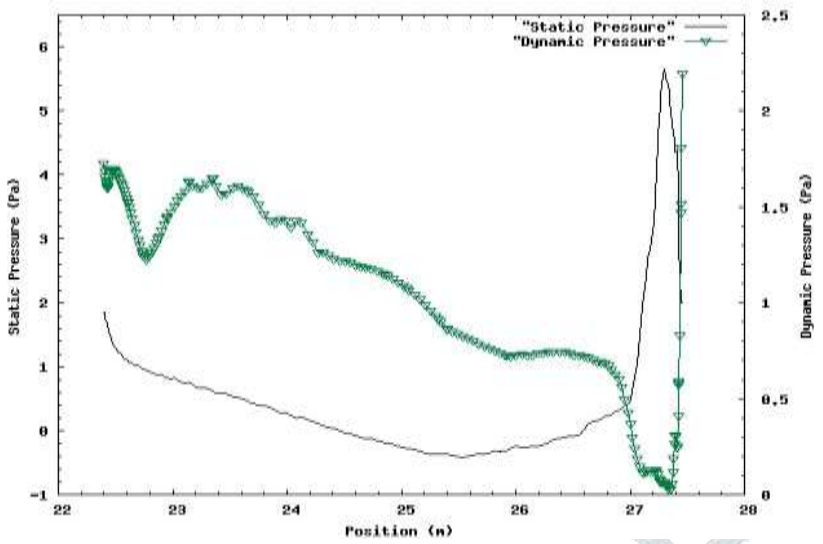

Figure 7: Pressure variation along the length of lowered section of the pipe.

4 Conclusions and future work

A 3D-CFD model has been developed for the generation of hydrates in gas pipes. So far, the findings are in line with previous research on the condensation and buildup of liquid water regions in steep terrain pipelines produced by gravity. It was also possible to pinpoint critical hydrate formation locations. Overall, fairly plausible theoretical explanations for the complex physical occurrence could be found.

Unfortunately, no direct comparison with experimental results has been possible so far due to a lack of data. However, this will be the subject of a future paper. Model validation measurements are now being carried out in a real hilly terrain pipeline. In the future, a precise kinetic model will be used to mimic the influence of hydrate nucleation and growth events on a macroscopic scale.

References

[1] J.J. Carroll, *Natural Gas Hydrate: A Guide for Engineers*. Elsevier Science, 2003.

[2] E.D. Sloan & K.A. Koh, *Clathrate Hydrates of Natural Gases*, 2008.

[3] W.M. Deaton & E.M. Frost, Jr., Gas hydrates and their relation to the operation of natural-gas pipe lines. Technical report, United States Department of the Interior, Bureau of Mines, July 1946.

[4] P.Raj Bishoni & V. Natarajan, Formation and decomposition of gas hydrates. *Fluid Phase Equilibria*, **117**, pp. 168–177, 1996.

[5] C.P. Ribeiro Jr. & P.L.C. Lage, Modelling of hydrate formation kinetics: State-of-the-art and future directions. *Chemical Engineering Science*, **63(8)**, pp. 2007–2034, 2008.

[6] UBC, https://circle.ubc.ca/bitstream/handle/2429/1133/5434.pdf.

[7] UT, http://www.tuhfp.utulsa.edu/.

[8] S.R. Davies, J.A. Boxall, L.E. Dieker, A.K. Sum, C.A. Koh, E.D. Sloan, J.L. Creek & Z.-G. Xu, Predicting hydrate plug formation in oil-dominated flowlines. *Journal of Petroleum Science and Engineering*, **72(3-4)**, pp. 302– 309, 2010.

[9] *Fluent 6.3 Users Guide*.

[10] B.V. Balakin, A.C. Hoffmann & P. Kosinki, Experimental study and computational fluid dynamics modeling of deposition of hydrate particles in a pipeline with turbulent water flow. *Chemical Engineering Science*, 22 November 2010.

[11] S.C.K. De Schepper, G.J. Heynderickx & G.B. Marin, Modeling the evaporation of a hydrocarbon feedstock in the convection section of a steam cracker. *Computers & Chemical Engineering*, **33(1)**, pp. 122–132, 2009.

[12] A. Alizadehdakhel, M. Rahimi & A.A. Alsairafi, Cfd modeling of flow and heat transfer in a thermosyphon. *International Communications in Heat and Mass Transfer*, **37(3)**, pp. 312–318, 2010.

[13] Y.F. Makogon, *Hydrates of Hydrocarbons*. PennWell Books, 1997.

[14] D. Kashchiev and A. Firoozabadi, Nucleation of gas hydrates. *Journal of Crystal Growth*, **243(3-4)**, pp. 476–489, 2002.

[15] P. Mills, Non-Newtonian behaviour of flocculated suspensions. *J. Phys. Lett.*, **46**, pp. L301–L309, 1985.